Ultrafast Analog Fourier Transform Using 2-D *LC* Lattice

Ehsan Afshari, *Member, IEEE*, Harish S. Bhat, and Ali Hajimiri, *Member, IEEE*

***Abstract*—We describe how a 2-D rectangular lattice of inductors and capacitors can serve as an analog Fourier transform device, generating an approximate discrete Fourier transform (DFT) of an arbitrary input vector of fixed length. The lattice displays diffractive and refractive effects and mimics the combined optical effects of a thin-slit aperture and lens. Diffraction theories in optics are usually derived for 3-D media, whereas our derivations proceed in 2-D. Analytical and numerical results show agreement between lattice output and the true DFT. Potentially, this lattice can be used for an extremely low latency and high throughput analog signal processing device. The lattice can be fabricated on-chip with frequency of operation of more than 10 GHz.**

***Index Terms*—Discrete Fourier transforms, lattice circuits, physical theory of diffraction, planar transmission lines, ultra-fast analog signal processing.**

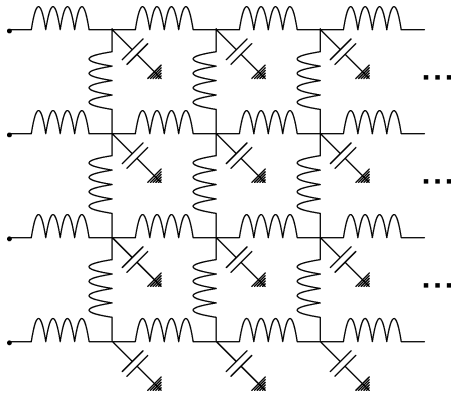

Fig. 1. 2-D lattice of inductors and capacitors (2-D *LC* lattice).

I. Introduction

THE 2-D lattices of inductors and capacitors (2-D *LC* lattices), an example of which is diagrammed in Fig. 1, are a natural generalization of 1-D transmission lines. In our earlier work [1], general models for 2-D *LC* lattices were derived, starting from Kirchhoff's laws of voltage and current. These models consist of partial differential equations (PDEs) arising from continuum and quasi-continuum limits, which are valid for signals with frequency content below a certain threshold value. Based on the PDE models and numerical simulations, it was found that a 2-D *LC* lattice could be used as a power combiner. Such a lattice has been designed and fabricated on chip [2] in a 0.13 μm SiGe BiCMOS process, where it has been used to implement a power amplifier that generates 125 mW at 85 GHz.

Here we apply a combination of continuum modeling, scalar diffraction theory, and numerical simulation to demonstrate that 2-D *LC* lattices can generate approximate Fourier transforms of input signals. Let us be more specific about this claim. Suppose we are given an input vector of length M, denoted by $\mathbf{x} \in \mathbb{R}^M$. In this case, we work with a 2-D *LC* lattice that has N nodes in the horizontal direction and M nodes in the vertical direction. For definiteness, in this paper we use (1,1) and (N, M) to denote, respectively, the lower-left and upper-right corners of the lattice. We drive the left boundary of the lattice with the voltage

$$V_{1,j}(t) = \alpha_1 x_j \sin(2\pi\omega t), \qquad 1 \le j \le M$$

where α_1 is an appropriate scaling factor, x_j is the j-th component of the input vector $\mathbf{x}$, and ω is an appropriate carrier frequency. Later in this paper we describe how to choose the lattice inductances L_{ij} and capacitances C_{ij} in a certain way, to take advantage of electrical analogues of optical phenomena such as refraction and diffraction. Our claim is that in such a lattice, the voltage at the right boundary will take the form

$$V_{N,j}(t) = \alpha_2 y_j \sin(2\pi\omega t), \qquad 1 \le j \le M.$$

Here α_2 is an appropriate scaling factor, and y_j is the j-th component of the output vector $\mathbf{y}$, which will turn out to be an approximation of the exact discrete Fourier transform of $\mathbf{x}$, i.e., $\mathbf{y} \approx \mathrm{DFT}(\mathbf{x})$. We may think of $\mathbf{y}$ and $\mathrm{DFT}(\mathbf{x})$ as M-vectors of phasors, or, equivalently, as elements of the complex vector space $\mathbb{C}^M$.

A. Methodology and Merits

As mentioned, our solution takes advantage of the connection between 2-D *LC* lattices in optics. For waves with sufficiently large wavelength, Kirchhoff's laws of voltage and current for a 2-D *LC* lattice can be approximated very well by a continuum model consisting of the scalar wave equation. The same PDE arises in the context of optics; starting from this PDE, the theories of Kirchhoff, Sommerfeld, Fresnel, and Huygens show that

Manuscript received December 9, 2006; revised . First published February 8, 2008; current version published September 17, 2008. This paper was recommended by Associate Editor A. G. Andreou.

E. Afshari is with the Department of Electrical and Computer Engineering, Cornell University, Ithaca, NY 14853 USA (e-mail: ehsan@ece.cornell.edu).

H. S. Bhat is with the School of Natural Sciences, University of California, Merced, CA 95344, USA.

A. Hajimiri is with the Department of Electrical Engineering, California Institute of Technology, Pasadena, CA 91125 USA.

Digital Object Identifier 10.1109/TCSI.2008.918151

a thin-slit diffraction aperture can be used to generate an analog Fourier transform of an image. Such theories assume, typically, that light propagates in a 3-D continuum such as air. In this paper, we present analytical and numerical results for thin-slit diffraction in a 2-D *LC* lattice. Together, these results indicate that by choosing lattice capacitance/inductance, lattice size, and input carrier frequency in a careful way, we can design 2-D *LC* lattices that generate analog Fourier transforms in the same way as a thin-slit diffraction aperture for 3-D optics.

This is almost the entire solution. Our analysis also indicates that, by itself, the output through a 2-D thin-slit diffraction suffers a phase shift that can be corrected using a lens. We show through numerical simulations that a 2-D *LC* lattice can be used to refract incoming waves, and therefore that such a lattice can be used as a lens. Our Fourier transform device, therefore, is effectively the superposition of a diffractive lattice with a lattice-based lens. The combination of these effects yields an in-phase analog Fourier transform.

Using a 2-D *LC* lattice as an approximate Fourier transform device has three distinct features. First, the latency of the device, defined as the time required for the input signal to propagate from the left to the right boundary, can be be extremely small. The latency is computed by multiplying the characteristic delay of the lattice, $\tau = \sqrt{LC}$, by the number of nodes in the horizontal direction. In today's Silicon processes, inductances of 30 pH and capacitances of 20 fF are achieveable; at values that are much smaller, parasitic effects become an issue. Therefore, the delay τ can be as low as 775 fsec for today's Silicon processes. As a rule of thumb, we find that to transform a vector with M components requires a lattice with roughly $N = (5/4)M$ nodes in the horizontal direction. As a function of M, the latency is $(5/4)M\tau$. Using a 2-D *LC* lattice, a vector of length 1024 could be transformed in less than 800 psec. Note that the latency is independent of the carrier frequency ω, and that it grows linearly in the size of the input vector M.

Second, the device throughput can be extremely high. One does not need to wait for an input signal to propagate all the way from the left boundary to the right boundary of the lattice before injecting a new, different input signal. Inputs could be stacked in time, and multiple Fourier transforms could be computed without waiting. Preliminary simulations indicate that the throughput of the lattice can reach 10 Gbits/sec.

Finally, design and fabrication is easier and less costly for *LC* lattices than for optical materials with similar properties.

B. Historical Remarks

Classic texts [3], [4] on wave and Fourier optics concentrate their efforts on 3-D media, ostensibly because most experimental diffraction setups involve light propagation in three spatial dimensions. However, the propagation of light in 2-D media has been considered before. Diffraction integrals for a 2-D dispersion-free continuum were almost surely known to Sommerfeld—see, for example, equations (2.23)–(2.26) of Bouwkamp's survey article [5] and references therein. Recent work in this area is due to J. J. Stamnes [6]–[10], who has derived exact, approximate, and numerical results for focusing and diffraction of 2-D waves. Stamnes' results stop short of showing that even for 2-D waves, a standard Fourier transform integral can be derived. Furthermore, Stamnes' work deals exclusively with waves propagating through a dispersionless continuum, which describes our discrete 2-D *LC* lattice only approximately, and only in certain frequency regimes. Other papers on 2-D diffraction [11], [12] do not differ in this regard.

Our work owes a great deal to the classical approaches of Sommerfeld and Kirchhoff, also employed by Stamnes. Their approach for single-slit diffraction problems consists primarily in using one of Green's identities to express the diffracted field at a point P_0 in terms of a particular integral around a curve centered at P_0. Denote this integral by $I(P_0)$. Next, assume that the spatial part of the diffracted field is a solution of the Helmholtz equation

$$(\nabla^2 + k^2)\psi = 0. \tag{1}$$

Knowledge of the radially symmetric solutions of (1), together with a choice of boundary conditions for the field and its normal derivative on the aperture of the slit, enables us to pass from the integral $I(P_0)$ to a diffraction integral. In the present work, we validate our numerical results on diffraction using this classical approach.

The main alternative to the Kirchhoff-Sommerfeld approach outlined above is the geometric or ray theory of diffraction due to Keller [13], [14] and his collaborators. Application of Keller's elegant methods to the context of 2-D *LC* lattices shall have to wait until a future publication.

Finally, let us note that the classical work [15] of Brillouin on crystal lattices makes explicit the analogy between crystal lattices, mass-spring models, and *LC* lattices in one, two, and three spatial dimensions. Brillouin's primary focus in this work was the development of bandgap theories for lattices with periodic inhomogeneities. The lattice inhomogeneities we consider are of an entirely different type.

C. Main Results

In this paper we present the following results.

1) A derivation of a phase-shifted Fourier transform integral for the illumination of a point source onto a plane screen. The derivation follows scalar diffraction theory for a thin slit in a 2-D medium.
2) A numerical demonstration that when lattice size equals a small number of wavelengths of the input carrier waves, a discrete 2-D *LC* lattice can be used as a diffraction aperture.
3) Numerical simulations that show that varying capacitance in a lens-shaped region in the center of the lattice effectively cancels the phase shift from the Fourier transform integral. These simulations indicate that the lattice can be used to compute approximate discrete Fourier transforms that match the true DFT quite well.

II. Lattice Equations and PDE Models

A. Kirchhoff's Laws

For a 2-D *LC* lattice that extends infinitely in both directions, Kirchhoff's laws of voltage and current read

$$I_{i,j-1/2} + I_{i-1/2,j} - I_{i+1/2,j} - I_{i,j+1/2} = C_{ij}\frac{d}{dt}V_{ij} \tag{2a}$$

and

$$V_{i,j-1} - V_{ij} = L_{i,j-1/2}\frac{d}{dt}I_{i,j-1/2} \tag{2b}$$

$$V_{ij} - V_{i+1,j} = L_{i+1/2,j}\frac{d}{dt}I_{i+1/2,j}. \tag{2c}$$

Here we have assumed that the capacitances C_{ij} and the inductances $L_{\alpha\beta}$ stay fixed as a function of time. Otherwise the right-hand sides of (2) would have to be modified, and the dynamics of the lattice would be nonlinear. In contrast, system (2) is linear.

B. Continuum Limit

In earlier work [1], the continuum limit of (3) was derived using standard Taylor series arguments. In the case of a uniform lattice, one can arrive at a continuum limit by examining the dispersion relation, a procedure we now describe. Take $C_{ij} = C$ and $L_{\alpha,\beta} = L$ everywhere, differentiate (2a) with respect to time, and then substitute (2b), (2c) to derive the single second-order equation for lattice voltage

$$LC\frac{d^2}{dt^2}V_{ij} = V_{i-1,j} + V_{i+1,j} + V_{i,j-1} + V_{i,j+1} - 4V_{i,j} \tag{3}$$

Assume that the spacing between lattice elements is the same in both x and y direction, and denote this constant lattice spacing by d. Substituting

$$V_{i+1,j}(t) = e^{ik_x d}V_{i,j}(t)$$
$$V_{i,j+1}(t) = e^{ik_y d}V_{i,j}(t)$$
$$V_{i,j}(t) = e^{-i\omega t}$$

one derives the discrete dispersion relation

$$\omega_d = \frac{2}{\sqrt{LC}}\left[\sin^2\frac{k_x d}{2} + \sin^2\frac{k_y d}{2}\right]^{1/2}. \tag{4}$$

When $\theta \ll 1$, we may approximate $\sin\theta \approx \theta$. Therefore, when $k_x d \ll 1$ and $k_y d \ll 1$, we have that ω_d may be approximated by $\omega = d(LC)^{-1/2}[k_x^2 + k_y^2]^{1/2}$. Replace L by $d\ell$ and C by dc, where ℓ and c are, respectively, inductance and capacitance per unit length. Assuming that ℓ and c stay constant in the $d \to 0$ limit, we arrive at the *continuum* dispersion relation

$$\omega = \frac{1}{\sqrt{\ell c}}\left[k_x^2 + k_y^2\right]^{1/2} \tag{5}$$

which is the exact dispersion relation for the scalar wave equation

$$\ell c\frac{\partial^2 v}{\partial t^2} = \nabla^2 v. \tag{6}$$

In previous derivations [1], we started with (3), then posited a continuous function $v(x, y, t)$ such that $v(id, jd, t) \approx V_{ij}(t)$, expanded $V_{i+\sigma,j}$ and $V_{i,j+\sigma}$ in Taylor series about $V_{i,j}$, and thereby derived precisely the same PDE model (6). The derivation of (6) as a continuum model of (3) on the basis of exact/approximate dispersion relations has its own utility, as we now show.

C. Range of Validity

One wants to understand, quantitatively, where the continuum model (6), is valid. Suppose that an acceptable relative error in the approximation $\sin^2\theta \approx \theta^2$ is 3.0%—this is achieved for $|\theta| < 0.297$, giving us the conditions $k_x d < 0.297$ and $k_y d < 0.297$. Because wavelength is related to wave number by $\lambda = 2\pi/k$, the conditions on k_x and k_y imply

$$\frac{\lambda_x}{d}, \frac{\lambda_y}{d} > \frac{2\pi}{0.297} \approx 21.$$

As long as one wavelength occupies more than 21 lattice spacings, the continuum dispersion relation (5) and PDE (6) is a decent approximation to the fully discrete dispersion relation (4) and differential (3).

We may go further. For the sake of illustration, let us fix the inductance and capacitance to be, respectively, $L = 30$ pH and $C = 20$ fF. Suppose waves of frequency ω propagate through such a lattice, in the x direction only. In this case $k_y = 0$. The dispersion relation (4) may now be used to determine that, with these parameters

$$k_x d = 2\sin^{-1}\frac{\omega}{2.6 \times 10^{12}}.$$

Then $k_x d < 0.297$ as long as $\omega < 61$ GHz, the cutoff frequency for validity of the continuum model of the 2-D *LC* lattice. Note also that is easy to read off the cutoff frequency ω_{M} for the lattice itself from the above calculation

$$\omega_{\mathrm{M}} \approx 2.6 \times 10^{12}\ \mathrm{sec}^{-1} \approx 410\ \mathrm{GHz}.$$

D. Effect of Boundaries

Of course, experimentally realizable lattices must be of finite extent. Furthermore, when we numerically simulate the lattice equations, we must take into account appropriate boundary conditions that arise due to finiteness of the lattice. For these reasons we give a few details regarding Kirchhoff's laws on the boundaries.

For a finite lattice with M nodes in the x direction and N nodes in the y direction, we see that

$$\text{Equation(2a)holds for } 2 \le i \le M, 2 \le j \le N$$
$$\text{Equation(2}b\text{)holds for } 1 \le i \le M, 2 \le j \le N$$
$$\text{Equation(2}c\text{)holds for } 1 \le i \le M-1, 1 \le j \le N.$$

Equations (2b) and (2c) already take into account contributions due to voltage nodes on the boundary and need not be modified. Meanwhile, (2a) for $i = 1$, $i = M$, $j = 1$, and $j = N$ must be corrected by deleting those terms on the left-hand side corresponding to edges outside the lattice. Furthermore, we assume the right boundary of the lattice is resistively terminated with resistors obeying Ohm's law, so that the equations for $i = M$ read

$$C_{M,j}\frac{d}{dt}V_{M,j} = I_{M,j-1/2} + I_{M-1/2,j} - I_{M+1/2,j} - V_{M,j}R_j^{-1}$$

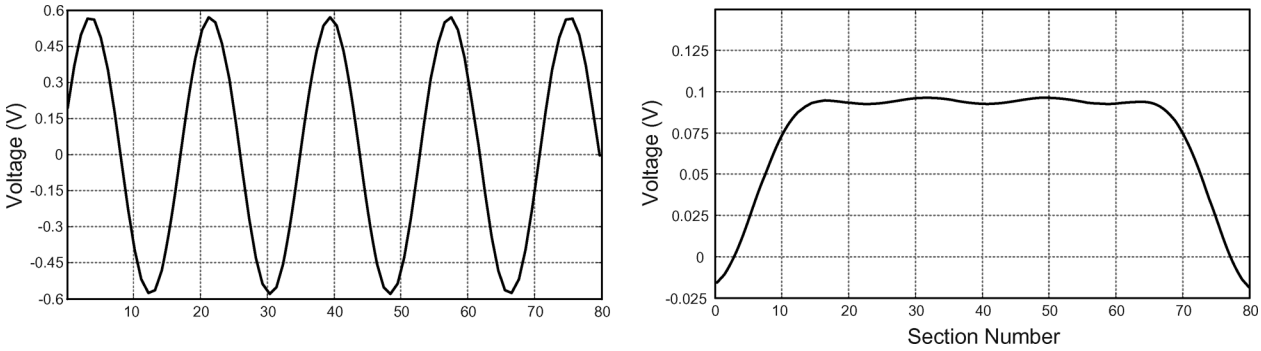

Fig. 2. Simulation of a uniform 2-D *LC* lattice showing diffractive effects. The input signal is our choice of forcing function at the left boundary of the lattice, and the output signal is the signal at the right boundary of the lattice. The forcing is sinusoidal and given by (7), with $\omega = 60$ GHz. Lattice inductances are $L = 30$ pH and lattice capacitances are $C = 20$ fF.

with the convention that $I_{M,j-1/2} = 0$ for $j = 1$ and $I_{M+1/2,j} = 0$ for $j = N$. The resistances R_j are chosen to minimize the reflection coefficient for waves incident on the right boundary. This is a basic impedance matching problem, and for a uniform medium the solution is given by choosing $R = \sqrt{L/C}$ everywhere along the right boundary.

E. A Hypothesis

Suppose we construct a finite, rectangular 2-D *LC* lattice with L and C as mentioned above, and suppose we drive the left boundary at a frequency of 60 GHz. In this case, the wave (6) is a good continuum model, leading us to the following hypothesis: *it should be possible to observe in a 2-D LC lattice all those effects predicted by scalar theories of light—especially scalar diffraction and refraction—assuming that relevant parameters have been chosen in such a way that the continuum model is good*. In what follows, we show the validity of this hypothesis.

III. Diffraction: Theory

Let us turn our attention to waves with wavelength sufficiently large so that only a few wavelengths fit in the finite lattice. In this situation, we claim that the lattice acts as a diffraction slit. To give a definite example, consider a 100×80 lattice where we drive the left boundary as follows:

$$V_{1,j}(t) = 0.5 \sin(\beta j) \sin(2\pi\omega t). \tag{7}$$

Take the lattice parameters to be $L = 30$ pH and $C = 20$ fF, and take the driving frequency to be $\omega = 60$ GHz. Then the lattice dispersion relation implies that for a wave propagating only in the x-direction, slightly less than five wavelengths of the wave fit inside the 100×80 lattice. Of course, if the forcing is of the form (7), then the wave will *not* propagate in the x-direction only. Parts of the wave will reflect off the top and bottom boundaries of the lattice in ostensibly complicated ways, and we would not expect the outgoing signal, $V_{100,j}(t)$, to look anything like the original input signal. The question is: what will the output look like?

To try to guess the answer without any calculations, consider that the problem of squeezing a long wave through a narrow opening is really just a thin-slit diffraction problem. We are about to consider the problem of two uniform 2-D continuous media separated by a thin 1-D slit, where the slit is just a few wavelengths wide. Waves propagating from left to right through the slit are diffracted, and one can develop a Huygens–Fresnel type theory to predict the illumination far to the right of the aperture, due to a source to the left of the aperture. Roughly speaking, the illumination will be a phase-shifted Fourier transform of the source.

Going back to the 100×80 lattice with the above choice of parameters and the sinusoidal forcing (7), Fig. 2 shows what we see from a numerical simulation of the 2-D *LC* lattice (2).

The input is a sinusoidal function of the vertical coordinate j, and the output is clearly a different sort of function altogether. It turns out that the output is a phase-shifted or "blurry" version of the 1-D Fourier transform of the input. Eventually we will show simulations of a lattice with the same parameters except inside a lens-shaped region in the lattice interior. The lens will cancel out the phase shift and bring the Fourier transform into focus.

Before discussing these simulations, let us take a moment to develop the elementary theory of scalar diffraction for 2-D waves. Though derivations of Kirchhoff and Rayleigh–Sommerfeld diffraction integrals have appeared in the literature before, we offer our own derivations here. This is in part because diffraction of 2-D waves has not attracted much attention in the literature, and the reader may not be fully aware of the near- and far-field Hankel function asymptotics necessary to proceed in this case.

We begin by proving a Green's identity that forms the cornerstone of the 2-D wave theory of diffraction. Suppose we have a 2-D domain Ω, as in Fig. 3.

Assume that U is a scalar field that satisfies the Helmholtz equation

$$(\nabla^2 + k^2)U = 0$$

Given a point $P_0 \in \Omega$, we want to relate $U(P_0)$ to the values of U on the boundary of Ω, which we label as $\partial\Omega$. Use Green's Theorem (with U, G as solutions of the Helmholtz equation) which says

$$\iint_{\Omega} U\nabla^2 G - G\nabla^2 U ds = \iint_{\partial\Omega} U\frac{\partial G}{\partial n} - G\frac{\partial U}{\partial n} dl.$$

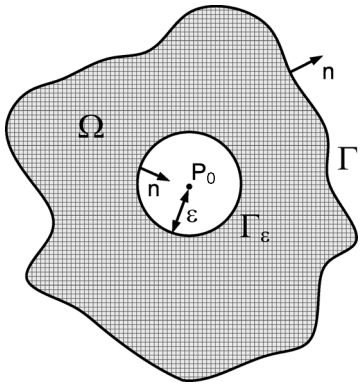

Fig. 3. Setup for deriving Green's function representation of $U(P_0)$.

Because $\nabla^2 G = -k^2 G$ and $\nabla^2 U = -k^2 U$, the left-hand side of the above equation is zero, i.e.,

$$\iint_{\Omega} U(-k^2 G) - G(-k^2 U) ds = 0.$$

The boundary of Ω is the sum of two curves Γ and Γ_ϵ. The outer curve Γ is smooth but otherwise arbitrary. The inner curve Γ_ϵ is a circle of radius ϵ with center P_0. Green's Theorem says

$$0 = \int_{\partial\Omega} U\frac{\partial G}{\partial n} - G\frac{\partial U}{\partial n} dl$$

and because

$$\partial\Omega = \Gamma + \Gamma_\epsilon$$

this implies

$$-\int_{\Gamma_\epsilon} U\frac{\partial G}{\partial n} - G\frac{\partial U}{\partial n} dl = \int_{\Gamma} U\frac{\partial G}{\partial n} - G\frac{\partial U}{\partial n} dl. \tag{8}$$

We evaluate the left integral, using the fact that on the curve Γ_ϵ, we have $dl = \epsilon d\theta$. We set $G(r)$ equal to the radially symmetric solutions of the 2-D Helmholtz equation. These are solutions of the equation

$$\frac{1}{r}\frac{\partial}{\partial r}\left(r\frac{\partial G}{\partial r}\right) + k^2 G = 0$$

which is in fact Bessel's equation. Solutions of Bessel's equation are Hankel functions, i.e.,

$$G(r) = H_0(kr) = J_0(kr) + iY_0(kr)$$

where J_0 is a Bessel function of the first kind and Y_0 is a Bessel function of the second kind. Then, denoting the left-hand side of (8) by S_L, we have

$$S_L = -2\pi\epsilon\left(-kU(P_0+\epsilon)\frac{\partial H_0}{\partial r}(k\epsilon) - H_0(k\epsilon)\frac{\partial U}{\partial n}\right)$$

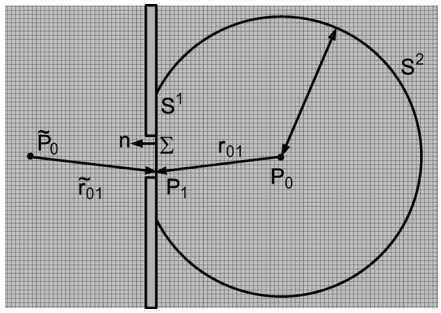

Fig. 4. Setup for deriving Rayleigh–Sommerfeld diffraction integral.

$$\approx -2\pi\epsilon\left(-kU(P_0)\left(-\frac{k\epsilon}{4} + i\frac{2}{\pi}\frac{1}{k\epsilon}\right) - \left(1 + i\frac{2}{\pi}\log\left(\frac{k\epsilon}{2}\right)\right)\right) \tag{9}$$

where we have made the approximations

$$H_0(k\epsilon) \approx 1 + i\frac{2}{\pi}\log\left(\frac{k\epsilon}{2}\right)$$
$$\frac{\partial}{\partial r}H_0(k\epsilon) \approx -\frac{k\epsilon}{4} + i\frac{2}{\pi}\frac{1}{k\epsilon}.$$

These approximations are valid for $\epsilon \ll 1$, and the right- and left-hand sides of (9) have the same asymptotic behavior in the $\epsilon \to 0$ limit. However, the $\epsilon \to 0$ limit of the right-hand side of (9) is easily computable, leading to the result

$$\lim_{\epsilon\to 0}\left[-\int_{\Gamma_\epsilon} U\frac{\partial G}{\partial n} - G\frac{\partial U}{\partial n} dl\right] = 4iU(P_0).$$

Using this result in (8), we write

$$U(P_0) = \frac{1}{4i}\int_{\Gamma} U\frac{\partial G}{\partial n} - G\frac{\partial U}{\partial n} dl. \tag{10}$$

A. Rayleigh–Sommerfeld

Consider diffraction in 2-D from a screen with aperture Σ as in Fig. 4.

We now use the integral formula (10) to compute $U(P_0)$ with $\Gamma = S^1 + S^2$. We break the integral over Γ into two pieces, i.e.,

$$U(P_0) = \frac{1}{4i}\int_{S^1} U\frac{\partial G}{\partial n} - G\frac{\partial U}{\partial n} dl + \frac{1}{4i}\int_{S^2} U\frac{\partial G}{\partial n} - G\frac{\partial U}{\partial n} dl. \tag{11}$$

First we do the integral over S^2 and give a condition under which it vanishes. We make use of the following approximations, valid for $R \gg 1$

$$G(R) = H_0(kR) \approx \sqrt{\frac{2}{\pi kR}}\exp\left[i(kR - \pi/4)\right]$$
$$\frac{\partial G}{\partial R} = k\frac{\partial}{\partial r}H_0(kR) \approx k\sqrt{\frac{2}{\pi kR}}i\exp\left[i(kr - \pi/4)\right].$$

Using these approximations, one derives

$$\begin{aligned}\int_{S^2} U\frac{\partial G}{\partial n} - G\frac{\partial U}{\partial n}dl &= \int_{S^2} Uk\sqrt{\frac{2}{\pi kR}}i\exp\left[i(kr-\pi/4)\right] \\ &\quad - \sqrt{\frac{2}{\pi kR}}\exp\left[i(kR-\pi/4)\right]\frac{\partial U}{\partial n}dl \\ &= \sqrt{\frac{2}{\pi k}}\int\sqrt{R}\left(ikU - \frac{\partial U}{\partial n}\right) \\ &\quad \times \exp\left[i(kR-\pi/4)\right]d\theta.\end{aligned}$$

The 2-D Sommerfeld outgoing radiation condition follows: if, for all θ

$$\lim_{R\to\infty}\left[\sqrt{R}\left(ikU - \frac{\partial U}{\partial n}\right)\right] = 0$$

then the S^2 integral vanishes, and the only contribution to the integral comes from S^1. That is, formula (11) reduces to

$$U(P_0) = \frac{1}{4i}\int_{S^1} U\frac{\partial G}{\partial n} - G\frac{\partial U}{\partial n}dl. \tag{12}$$

At this point, one must choose a Green's function G and boundary conditions for U, and it is here that the theories of Kirchhoff, Debye, and Rayleigh–Sommerfeld diverge. Although it is certainly possible to follow all of these paths in the 2-D case, we pursue the calculation only in the first Rayleigh–Sommerfeld case. That is, we take $G = G_-$ to vanish on all of S^1 by choosing

$$G_{=}H_0(kr_{01}) - H_0(k\tilde{r}_{01}). \tag{13}$$

See Fig. 4 for the meanings of r_{01} and $\tilde{r}_{01}$—these vectors are simply reflections of each other across the aperture Σ. The point $\tilde{P}_0$ to the left of Σ is the mirror image of the point P_0 to the right of Σ. In what follows, the outward unit normal points to the left from Σ. We stipulate the boundary condition that U vanishes on S^1 not including Σ; using this boundary condition and (13), we find that (12) reduces to

$$U_I(P_0) = \frac{1}{4i}\int_{\Sigma} U\frac{\partial G_-}{\partial n}dl.$$

Note that

$$\begin{aligned}\frac{\partial G_-}{\partial n} &= k\frac{\partial}{\partial r}H_0(kr_{01})\cos(\mathbf{n},\mathbf{r}_{01}) - k\frac{\partial}{\partial r}H_0(k\tilde{r}_{01})\cos(\mathbf{n},\tilde{\mathbf{r}}_{01}) \\ &= -kH_1(kr_{01})\cos(\mathbf{n},\mathbf{r}_{01}) + kH_1(k\tilde{r}_{01})\cos(\mathbf{n},\tilde{\mathbf{r}}_{01}).\end{aligned}$$

On Σ, we know that $\cos(\mathbf{n},\tilde{\mathbf{r}}_{01}) = -\cos(\mathbf{n},\mathbf{r}_{01})$ and that $r_{01} = \tilde{r}_{01}$. Therefore

$$\frac{\partial G_-}{\partial n} = -2k\cos(\mathbf{n},\mathbf{r}_{01})H_1(kr_{01}).$$

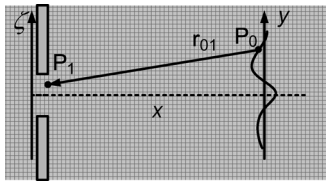

Fig. 5. Huygens–Fresnel picture showing illumination on a line several wavelengths away from the thin slit diffraction aperture.

This implies

$$U_I(P_0) = -\frac{k}{2i}\int_{\Sigma} U\cos(\mathbf{n},\mathbf{r}_{01})H_1(kr_{01})dl. \tag{14}$$

This is the 2-D version of the first Rayleigh–Sommerfeld diffraction integral.

B. Huygens–Fresnel

Our goal here is to determine the illumination onto a plane screen located several wavelengths away from the aperture. For diffraction problems in two spatial dimensions, we do not believe this calculation has appeared previously in the literature. The picture is given in Fig. 5. Starting from the diffraction integral (14), we note that inside the aperture Σ, we have $\cos\theta = x/r_{01}$. This gives

$$U_I(y) = -\frac{kx}{2i}\int_{\Sigma} U(\xi)\frac{H_1(kr_{01})}{r_{01}}d\xi.$$

We use $r_{01}^2 = x^2 + (y-\xi)^2$ and approximate

$$\begin{aligned}r_{01} &= x\sqrt{1+\left(\frac{y-\xi}{x}\right)^2} \\ &\approx x\left(1+\frac{1}{2}\left(\frac{y-\xi}{x}\right)^2\right) = x + \frac{1}{2}\frac{(y-\xi)^2}{x}.\end{aligned}$$

The same approximation strategy gives

$$\begin{aligned}\frac{1}{r_{01}} &\approx \frac{1}{x}\frac{1}{1+(y-\xi)^2/(2x^2)} \\ &\approx \frac{1}{x}\left(1-\frac{1}{2}\frac{(y-\xi)^2}{x^2}\right) = \frac{1}{x} - \frac{1}{2}\frac{(y-\xi)^2}{x^3}.\end{aligned}$$

The difference between the approximations of r_{01} and r_{01}^{-1} is that the $O(y-\xi)^2$ term appears in r_{01}^{-1} with an extra factor of x^{-2}. Since x is assumed large compared with the wavelength, we keep the $O(y-\xi)^2$ term only when r_{01} appears in the numerator, and drop it whenever r_{01} appears in the denominator. This gives

$$U_I(y) = \frac{-k}{2i}\int_{\Sigma} U(\xi)H_1\left[kx\left(1+\left(\frac{y-\xi}{x}\right)^2\right)\right]d\xi.$$

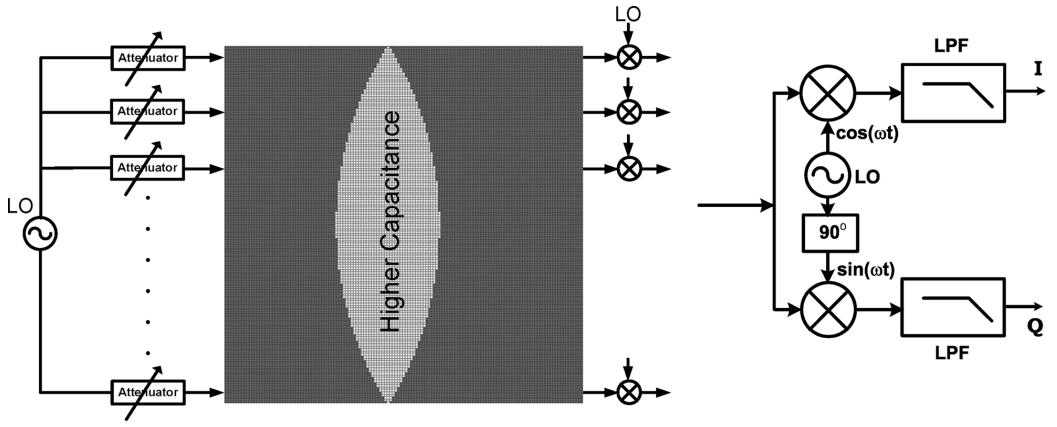

(a) Overall architecture (b) In-phase/Quadrature extraction

Fig. 6. Device architecture, showing output nodes that capture either the (a) amplitude or (b) phase and amplitude of the output Fourier transform. (a) Overall architecture. (b) In-phase/Qaudrature extraction.

Now we use the far-field asymptotics of the Hankel function to approximate

$$H_1\left[kx\left(1+\left(\frac{y-\xi}{x}\right)^2\right)\right] \approx \sqrt{\frac{2}{\pi}}\frac{e^{ikx}}{\sqrt{xk}}\exp\left[\frac{ik}{x}(y-\xi)^2-\frac{i\pi}{4}\right].$$

Inserting this approximation into the integral we have

$$U_I(y) \approx -\frac{k}{2i}\sqrt{\frac{2}{\pi}}\frac{e^{ikx}e^{-i\pi/4}}{\sqrt{kx}}\int_{\Sigma}U(\xi)\exp\left[\frac{ik}{x}(y-\xi)^2\right]d\xi$$
$$= C\sqrt{k}\frac{e^{ikx}}{\sqrt{x}}e^{\frac{ik}{x}y^2}\int_{-\infty}^{+\infty}\left\{U(\xi)e^{\frac{ik}{x}\xi^2}\right\}e^{-\left(\frac{2ik}{x}\right)y\xi}d\xi \quad (15)$$

where $U(\xi)=0$ when $\xi \notin \Sigma$, and where the constant $C = ie^{i\pi/4}/\sqrt{2\pi}$. Note that this last integral (15) is the Fourier integral with phase shift $\exp(ik\xi^2/x)$.

C. Interpretation

Let us interpret the result in Fig. 2 from the point of 2-D continuum diffraction theory just developed. With the chosen values of L, C, and ω, the continuum limit of the 2-D lattice equations is valid. The lattice used to produce Fig. 2 could fit about five wavelengths of the carrier wave. Suppose the lattice itself acts as a diffraction aperture—this would imply that the output should be given by (15), with $U(\xi)=\sin(\beta\xi)$ as the continuum version of the input (7). But unless there is some mechanism to cancel the phase shift $\exp(ik\xi^2/x)$, then the output will not be recognizable as anything close to the Fourier transform of $U(\xi)$. Qualitatively, this is precisely what we observed in Fig. 2.

In the next section, we provide numerical test results that show two things: 1) it is possible to cancel the phase shift by modifying the uniform 2-D *LC* lattice to incorporate a lens; 2) using this modified lattice, the diffracted output at the right boundary agrees quite well with the predicted Fourier transform.

IV. Diffraction: Numerics

A. Lens-Shaped Region

Fig. 6(a) shows one possible architecture of the circuit, with a lens-shaped region in the interior designed to cancel out the phase shift in the Huygens–Fresnel integral (15). The lens focuses the signal on the right (output) edge of the lattice; to choose lattice parameters such that the correct focal length is achieved, we used the thin lens formula (23) derived earlier. Note that the device shown in Fig. 6(a) outputs the amplitude of the Fourier transform; if we are interested in the phase information as well, we can extract it by using two mixers instead of one in each output node. The modification to each output node is diagrammed in Fig. 6(b). As shown, using in-phase and quadrature of the signal at each node, we can obtain phase and amplitude of the signal at each node. The trade-off is more complexity in the system (additional mixer and a 90-degree phase shifter in each node).

We defer further comments on the implementation to the end of this paper, and now demonstrate that, modified to include a built-in lens, the 2-D *LC* lattice can compute discrete Fourier transforms of input signals.

B. Fourier Transform

Direct numerical simulations show quite clearly the Fourier transform capabilities of the 2-D *LC* lattice. By this we mean that if the forcing of the lattice's left boundary is given by

$$V_{1,j}(t) = p_j \sin(2\pi\omega t) \quad (16)$$

then the signal at the right boundary will consist of an approximate, discrete Fourier transform of the spatial part $\mathbf{p}$ of the input signal. In what follows, all reported numerical results arise from solving Kirchoff's laws (2) for 80×100 lattices, subject to the boundary conditions described in Section II-D.

1) Sinusoidal Inputs: Fig. 7 shows the Fourier transform of two sinusoids, with two different spatial wavelengths.

The lattice parameters are nearly the same as before for Fig. 2: namely, outside the lens-shaped region shown in Fig. 6(a), we take $L = 30$ pH, $C = 20$ fF, and $\omega = 60$ GHz. Inside the lens-shaped region, we leave L unchanged but take $C = 60$ fF.

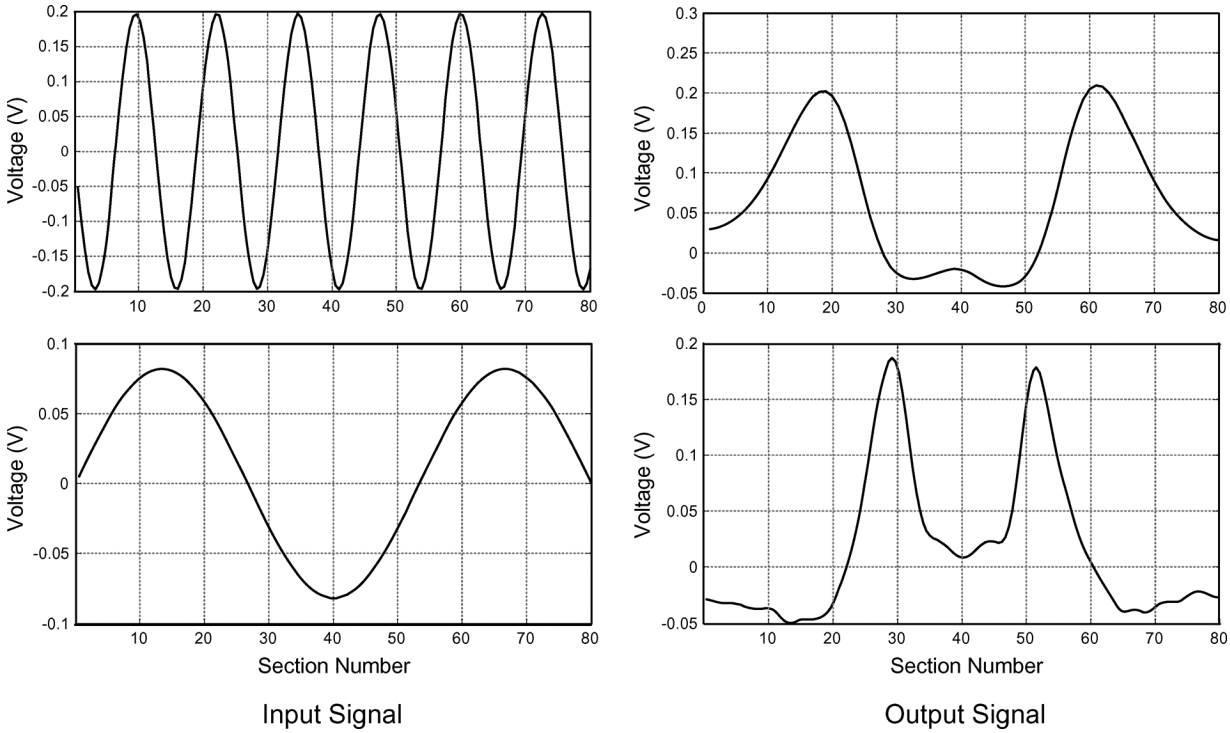

Fig. 7. Results for two different numerical simulations of the 2-D *LC* lattice showing how diffraction and lensing effects combine to effectively take the spatial 1-D Fourier transform of the input signal. The plots on the left (input signals) correspond to two different choices of p_j in expression (16), with $\omega = 60$ GHz. The plots on the right (output signals) show $V_{100,j}(t)$ as a function of vertical section number j, for a particular instant of time $t > 0$. Lattice parameters are $L = 30$ pH and $C = 20$ fF, except in a lens-shaped region in the center of the lattice where L is unchanged but $C = 60$ fF.

The lattice has 80 nodes in the vertical direction and 100 nodes in the horizontal direction. We force the left boundary with a sinusoidal forcing function of the form (7), and examine the output at the right boundary.

To ensure that the simulations are realistic, we add two effects not present in our mathematical analysis above. Namely, we add a mutual inductance term that takes into account coupling of adjacent inductors. As mentioned above, the coupling coefficient for this term is very small compared with unity (0.1), and the effect is not large. Furthermore, we assume each section as a resistance of 0.1Ω, and that all inductors and capacitors vary randomly by about 5% from the values reported above.

The output of the circuit shows clearly two peaks, as expected. Furthermore, the sinusoid with smaller wavelength (and therefore higher wave number) yields two peaks that are more widely separated than those generated by the sinusoid with larger wavelength (and therefore smaller wave number). Because the aperture of the lens is comparable with the wavelength of the input signal, diffractive effects are quite important. The output is *not* simply a focused version of the input, but a focused and diffracted version of the input. Comparing Fig. 2 and Fig. 7, it is now clear that the lens brings into focus the blurry Fourier transform that results from diffraction alone.

Finally, Fig. 7 clearly shows the dc value of the input. The first waveform has a lower average value compared to the second one and we can clearly see this difference in our output waveform.

2) Sinc Input: Next we consider the same lattice but with input equal to a sinc function

$$V_{1,j}(t) = 0.3\mathrm{sinc}(\beta j)\sin(2\pi\omega t). \tag{17}$$

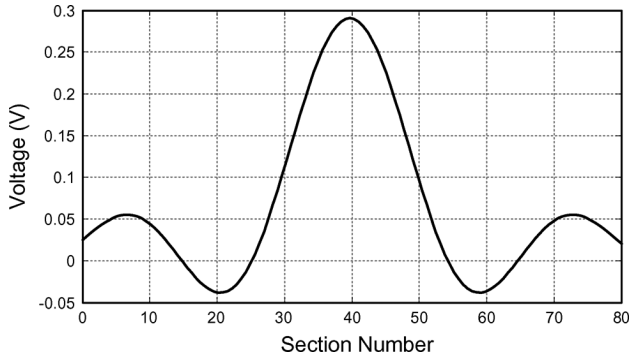

Fig. 8. The sinc input function corresponding to (17) with $\omega = 60$ GHz. The input $V_{1,j}(t)$ is plotted versus vertical section number j at a fixed instant of time t.

The input and output signals are shown, respectively, in Figs. 8 and 9.

The output is roughly symmetric, and roughly constant between elements 28 and 52. The true discrete Fourier transform, limited to a particular band of wave numbers, would be perfectly symmetric and have much steeper rise and fall sections than the curve shown in Fig. 9. However, given that we included just over two full cycles of the sinc function as input, the output is quite reasonable.

3) Step Input: Finally, we consider the same lattice but with input equal to a step function

$$V_{1,j}(t) = 0.15\sin(2\pi\omega t). \tag{18}$$

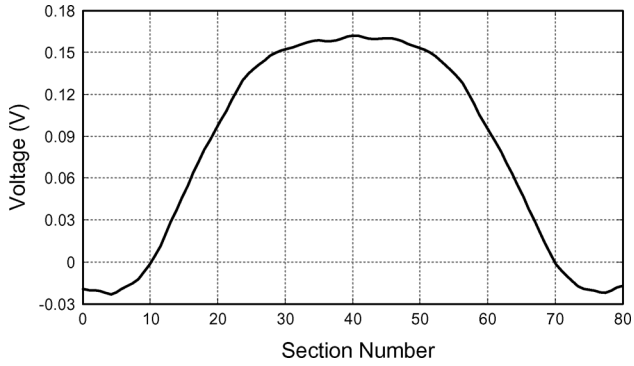

Fig. 9. Fourier transform of the sinc function in a 2-D *LC* lattice, showing the output $V_{100,j}(t)$ plotted versus vertical section number j, at a fixed instant of time t. Lattice parameters are unchanged from Fig. 7.

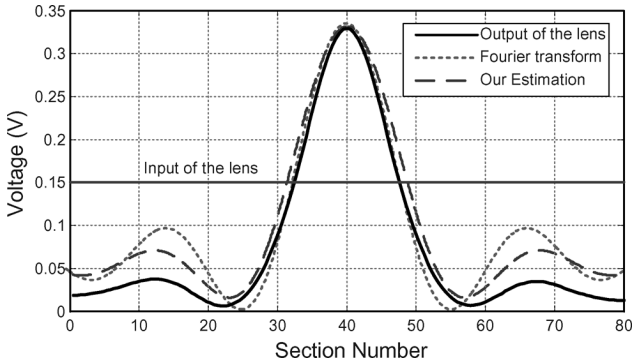

Fig. 10. Numerical simulation of the 2-D *LC* lattice (in black) as compared with our analytical prediction (in blue) and the true Fourier transform (in green) of the step function input given by (18), with $\omega = 60$ GHz. Lattice parameters are unchanged from Fig. 7. The black curve shows the numerically computed values of $V_{100,j}(t)$ as a function of vertical section number j, for a particular instant of time $t > 0$.

The output signal is shown in Fig. 10.

The Fourier transform of the step input is a sinc function, shown by the green curve. Our mathematical analysis predicts that the output should be given by the blue curve, while the numerical simulation itself yielded the black curve.

The three curves are qualitatively the same except in the tails, where there is some discernible disagreement. In the tails, one finds that our analysis is closer to the numerical simulation than the true Fourier transform. The error in the tails is due to two factors: 1) due to boundary effects, the finite lattice is not exactly the same as a thin slit diffraction problem, though it features qualitatively identical physics; 2) the lens-shaped region in the middle of the 2-D *LC* lattice is too thick for the paraxial approximation, explained later in (23), to be perfectly accurate. Better results can be obtained by modifying the Green's function $H_0(kr)$ and taking into account lens thickness, issues that we intend to explore in future work.

V. Refraction

In the previous section, we presented results for a 2-D *LC* lattice with a lens-shaped region in the interior with higher capacitance. This lens-shaped region is intended to cancel out a phase shift that appeared in the Fourier integral (15). The purpose of this section is to discuss the theory and numerics for lattice refraction, to establish that lensing is indeed possible, as was assumed in the previous section.

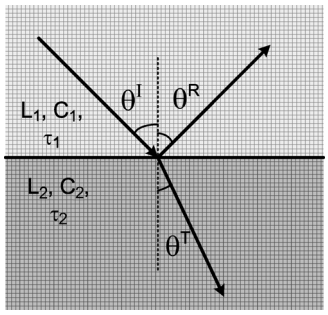

Fig. 11. Incident, reflected, and transmitted waves in a simple refraction problem.

A. Snell's Law

Fig. 11 shows the simplest scenario: a 2-D *LC* lattice with a jump in the delay, $\tau = \sqrt{LC}$, along a horizontal interface. That is to say, above the interface, the delay equals $\tau_1 = \sqrt{L_1 C_1}$, while below the interface, the delay equals $\tau_2 = \sqrt{L_2 C_2}$. The incident wave arrives from above at an angle θ^I and is partly reflected at an angle θ^R, and partly transmitted at an angle θ^T.

As derived earlier, the continuum model for the lattice is

$$\nabla^2 V = \tau^2 \frac{\partial^2 V}{\partial t^2} \tag{19}$$

where V is the voltage and $\tau = \sqrt{LC}$. By assuming that the incident, reflected, and transmitted waves are plane wave solutions of (19), propagating with the appropriate dispersion relation depending on whether they are in the upper or lower halves of the lattice, one can apply standard arguments to derive $\theta^I = \theta^R$, as well as Snell's law

$$\frac{\sin\theta^T}{\sin\theta^I} = \frac{\tau_1}{\tau_2}. \tag{20}$$

The derivation of (20) starting from (19) is completely standard [3], [4] and we shall not repeat it here.

B. Thick Parabolic Lens

Let

$$F(x,y) = x - \frac{\alpha}{2} y^2$$

so that the curve $F(x,y) = 0$ describes the left boundary of a parabolic lens. The right boundary of the lens is taken to be a vertical line as in Fig. 12. We take the delay outside the lens to be τ_1 and the delay inside the lens to be τ_2. Then the problem

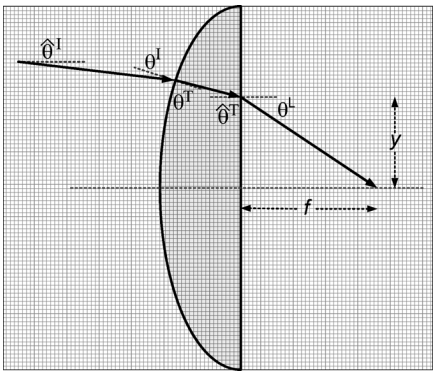

Fig. 12. Refraction problem for thick parabolic lens.

of determining the path of waves as they propagate through the lens can be solved by application of Snell's law.

Suppose we have a wave front propagating from left to right at angle $\hat{\theta}^I$, incident on the left boundary of the lens. The wave front's angle from the normal is given by

$$\theta^I = \hat{\theta}^I + \tan^{-1}(\alpha y).$$

Snell's law gives the angle of the transmitted wave

$$\sin\theta^T = \frac{\tau_1}{\tau_2}\sin\theta^I = \frac{\tau_1}{\tau_2}\sin\left(\hat{\theta}^I + \tan^{-1}(\alpha y)\right).$$

Of course, θ^T is the angle the transmitted wave front makes with the normal to the curved part of the lens. Subtracting off the contribution of this normal, we obtain

$$\begin{aligned}\hat{\theta}^T &= \theta^T - \tan^{-1}(\alpha y)\\ &= \sin^{-1}\left[\frac{\tau_1}{\tau_2}\sin\left(\hat{\theta}^I + \tan^{-1}(\alpha y)\right)\right] - \tan^{-1}(\alpha y). \quad (21)\end{aligned}$$

The angle $\hat{\theta}^T$ is the angle of incidence for the refraction problem at the right boundary of the lens. This is a consequence of the fact that the right boundary of the lens is vertical. Simple geometry shows that $y/f = \tan\theta^L$, where f is the focal distance. We apply Snell's law again to determine the angle of the outgoing wave that is transmitted through the right boundary of the lens

$$\sin\theta^L = \sin\hat{\theta}^T\frac{\tau_2}{\tau_1} \quad (22)$$

where $\hat{\theta}^T$ is given by (21).

C. Paraxial Approximation

Note that we can easily recover the paraxial approximation from the above formula for f. First set $\hat{\theta}^I = 0$. Next assume $\alpha \ll 1$, which converts all of the nonlinear functions $\tan$ and $\sin$ to the identity, i.e., if $q = O(\alpha)$, then $\tan q \approx q$, $\sin q \approx q$, and and likewise for the inverse functions. Starting with (22) and following the approximations through, one derives the thin lens or paraxial formula

$$f \approx \frac{y}{\left(1 - \frac{\tau_2}{\tau_1}\right)\alpha y} = \frac{1}{\alpha\left(1 - \frac{\tau_2}{\tau_1}\right)}. \quad (23)$$

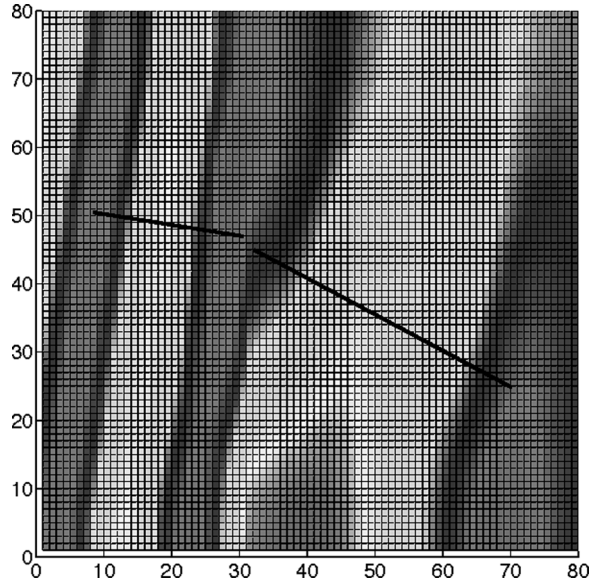

Fig. 13. Refraction in a 2-D *LC* lattice. The black lines show incident and refracted wave vectors predicted by Snell's law.

D. Numerics

We simulate the lattice by solving Kirchoff's laws (2) for an 80×80 lattice with boundary conditions given in Section II-D of this paper. For these simulations, we have one (or more) vertical interface separating two (or more) sections of the lattice. In certain sections of the lattice, we have $L_1 = 1$ nH and $C_1 = 1$ pF, while in other sections, we have $L_2 = L_1/\sqrt{10}$ and $C_2 = C_1/\sqrt{10}$. For the purposes of the following discussion, we define the following lattice delay constants:

$$\tau_1 = \sqrt{L_1 C_1} = 10^{-10.5}\ \text{sec}^{-1}$$
$$\tau_2 = \sqrt{L_2 C_2} = 10^{-11}\ \text{sec}^{-1}.$$

In all simulations that follow, the frequency in time of the boundary forcing is $\omega = 1$ G rad/s.

1) Snell's Law: For the first simulation, we take the lattice to have a single interface at $i = 30$. For $i < 30$, the delay is τ_1, while for $i > 30$, the delay is τ_2. Hence, the effective index of refraction is $\tau_1/\tau_2 = \sqrt{10}$. The incident angle, for the wave propagating from the left boundary towards the interface, is approximately $\theta^I \approx 0.149$ rad, and based on Snell's law we predict a transmitted angle $\theta^T \approx 0.488$ rad, which is what we see in the numerical simulation results displayed in Fig. 13.

The black lines are drawn to match the incident and refracted wave vectors, as predicted by Snell's law. Note that the black line in the $i > 30$ region is orthogonal to the numerically generated wavefronts. This implies that, in the direct numerical simulation, the angle that the refracted waves make with the normal to the interface is given quite accurately by Snell's law.

2) Plane Waves Refracted by a Slab: Next we examine a section of lattice with delay τ_2 sandwiched between two sections with delay τ_1. Here we take the incident angle to be zero, and note the change in wavelength of the wave as it propagates in the τ_2 section—see Fig. 14. Here the delay is τ_1 for $i < 20$ and

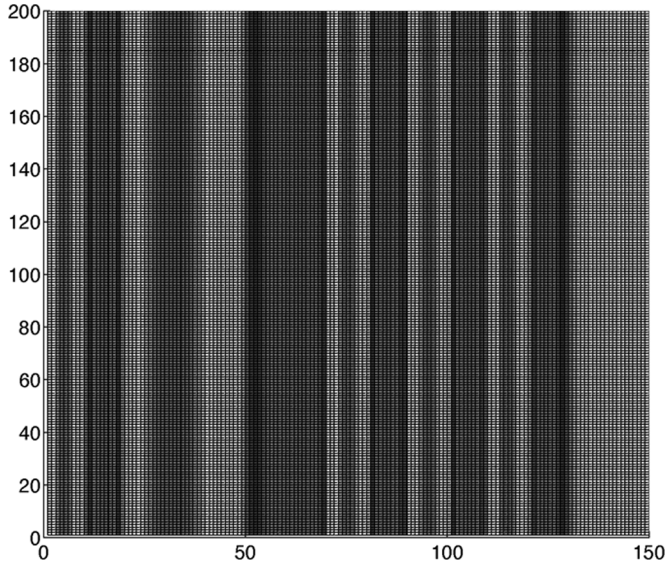

Fig. 14. Plane slab showing pure transmission and wavelength expansion in the $20 \leq i \leq 70$ section. The lattice delay equals τ_1 except inside the $20 \leq i \leq 70$ section, where the delay equals τ_2.

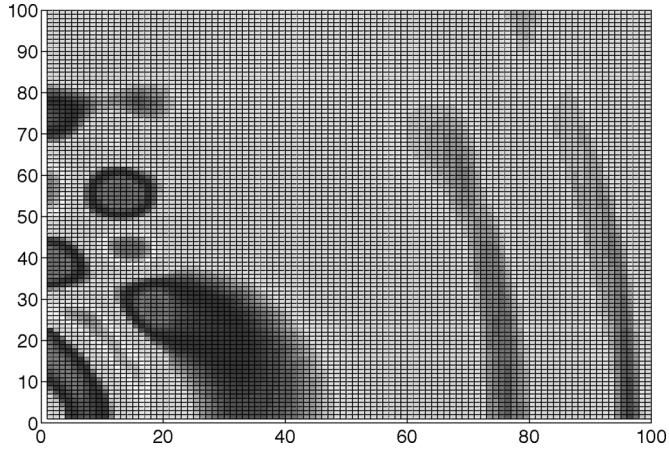

Fig. 15. Total internal reflection. At $t = 0$, voltage forcing is switched on along the left boundary at nodes $1 \leq j \leq 20$; resulting waves propagate at a sharp angle towards the interface at $i = 20$, where they undergo total internal reflection and are sent back towards the boundary at $i = 0$. The waves bounce repeatedly off the effective boundaries at $i = 0$ and $i = 20$ as they propagate upwards towards $j = 100$. The lattice delay equals τ_1 for $i < 20$ and equals τ_2 for $i > 20$.

$i > 70$, and the delay is τ_2 for $20 \leq i \leq 70$. Waves propagate from the left boundary towards the first interface at $i = 20$, undergo refraction and a change in wavelength, and continue propagating to the right until they are refracted again at the $i = 70$ interface, at which point their wavelength increases back to its original value. Impedance is matched at both interfaces so there is no reflection, i.e., there is no wave propagating from right to left from the interface back towards the left boundary.

3) Total Internal Reflection: Finally we present simulation results showing total internal reflection. Here the wave is launched from the left boundary and, more specifically, from the lower-left corner of the lattice consisting of the first 20 nodes $1 \leq j \leq 20$ on the left boundary. The nodes on the left boundary with $j > 20$ are left open, meaning that waves will reflect perfectly off those nodes. The wave propagates at an angle of roughly 56 degrees and hits the interface, located at $i = 20$. Because the effective index of refraction is $\sqrt{10}$, the critical angle for total internal reflection is approximately 18.5 degrees, so our incident angle is well beyond that. Fig. 15 shows clearly the wave bouncing off the $i = 20$ boundary at approximately $j = 30$, then propagating back towards the left $i = 0$ boundary, and then continuing to bounce off different boundaries as it propagates towards $j = 100$. The solution to the right of the interface, for $i > 20$, consists of an exponentially decaying evanescent wave.

VI. Conclusion

A. Implementation

It is feasible to make the 2-D *LC* lattice on a semiconductor substrate. Here we assume a Silicon substrate that is popular in today's technologies. We use pieces of metal as our inductors and metal-to-metal capacitances as the capacitors.

From the lattice dispersion relation (4), we know that in order to maximize the cutoff frequency, we need to minimize the values of inductors and capacitors in each section. However, we cannot arbitrarily shrink the capacitances of each section, because at some point, parasitic capacitance becomes comparable with our lumped capacitance. In today's typical Silicon processes, we can have inductances as low as 30 pH and capacitances as small as 5 fF before parasitic factors become an issue. The quality factor for these elements is around 20, giving us a cutoff frequency of around 300 GHz.

One important issue is ohmic loss of the Silicon substrate. To address this problem, we need to use a ground plane beneath our inductors to shield the Silicon substrate. By adding this layer, it is possible to achieve higher quality factors in our inductors. To find the exact value of inductance and capacitance as well as loss in each section, we use an E/M simulator such as Ansoft HFSS [16].

Another potential issue for this structure is magnetic coupling of the inductors. Adjacent inductors induce current in each other; to model this accurately requires additional terms in our circuit model (2). With typical values of inductors and capacitors, the effect of mutual inductance is very small: a careful E/M simulation shows that the coupling coefficient of adjacent inductors is less than 0.1.

Using the exact circuit models, we have simulated this structure and are in the process of fabricating the Fourier transform circuit in a SiGe BiCMOS process.

B. Conclusion and Future Directions

Numerical simulations indicate that 2-D *LC* lattices can be used to refract and diffract incoming waves of voltage. For waves with wavelength sufficiently large that only a few wavelengths are able to fit into a finite lattice, the lattice acts as a thin-slit diffraction aperture. By combining the lensing (refractive) and diffractive effects, we have demonstrated how a 2-D *LC* lattice can be used as a Fourier transform device.

These numerical findings were matched by our mathematical analysis of the refraction and diffraction problems for 2-D waves. In the case of diffraction, we found that a thin-slit aperture yields a phase-shifted Fourier transform, by way of the Huygens–Fresnel integral (15). Canceling out this phase shift

using a lens is precisely what the circuit shown in Fig. 6(a) is designed to do.

Simulations indicate that even in the presence of loss, mutual inductance, and capacitor/inductor variations, a 2-D *LC* lattice still manages to obtain discrete Fourier coefficients from the input signal. Furthermore, these Fourier coefficients match the true Fourier transform quite well.

The lattice erases the delay of digital gates, but not of sampling speed. Sampling is still required to read the output signal and pick up the Fourier coefficients. This and other implementation issues are currently being investigated. In future work, we hope to report measurement and test data for a Fourier transform device based on a 2-D *LC* lattice, fabricated on chip.

ACKNOWLEDGMENT

The authors would like to thank A. Komijani, M. Taghivand, and F. Bohn, California Institute of Technology, Pasadena, and B. Osting, Columbia University, New York, NY, for helpful discussions regarding this work.

REFERENCES

[1] E. Afshari, H. S. Bhat, A. Hajimiri, and J. E. Marsden, "Extremely wideband signal shaping using one- and two-dimensional nonuniform nonlinear transmission lines," *J. Appl. Phys.*, vol. 99, no. 5, p. 054901, 2006.

[2] E. Afshari, H. S. Bhat, X. Li, and A. Hajimiri, "Electrical Funnel: A new signal combining method," in *Proc. IEEE Int. Solid-State Circuits Conf. (ISSCC'06)*, San Francisco, CA, Feb. 2006, pp. 206–208.

[3] M. Born and E. Wolf, *Principles of Optics*, 7th ed. Cambridge, U.K.: Cambridge Univ. Press, 1999.

[4] J. W. Goodman, *Introduction to Fourier Optics*, 3rd ed. Greenwood Village, CO: Roberts, 2004.

[5] C. J. Bouwkamp, "Diffraction theory," *Rep. Prog. Phys.*, vol. 17, pp. 35–100, 1954.

[6] J. J. Stamnes, "Focusing of two-dimensional waves," *J. Opt. Soc. Am.*, vol. 71, no. 1, pp. 15–31, 1981.

[7] J. J. Stamnes, Waves in Focal Regions. Bristol, U.K., Hilger, 1986.

[8] J. J. Stamnes and H. A. Eide, "Exact and approximate solutions for focusing of two-dimensional waves—I: Theory," *J. Opt. Soc. Amer. A*, vol. 15, no. 5, pp. 1285–1291, 1998.

[9] H. A. Eide and J. J. Stamnes, "Exact and approximate solutions for focusing of two-dimensional waves—II: Numerical comparisons among exact, Debye, and Kirchhoff theories," *J. Opt. Soc. Amer. A*, vol. 15, no. 5, pp. 1292–1307, 1998.

[10] H. A. Eide and J. J. Stamnes, "Exact and approximate solutions for focusing of two-dimensional waves. III. Numerical comparisons between exact and Rayleigh–Sommerfeld theories," *J. Opt. Soc. Amer. A*, vol. 15, no. 5, pp. 1308–1319, 1998.

[11] A. C. Green, H. L. Bertoni, and L. B. Felsen, "Properties of the shadow cast by a half-screen when illuminated by a Gaussian beam," *J. Opt. Soc. Amer.*, vol. 69, no. 11, pp. 1503–1508, 1979.

[12] S. L. Dvorak and H.-Y. Pao, "A new solution for the problem of plane wave diffraction by a 2-D aperture in a ground plane," *IEEE Trans. Antennas Propagat.*, vol. 53, no. 7, pp. 2299–2306, Jul. 2005.

[13] J. B. Keller, "Diffraction by an aperture," *J. Appl. Phys.*, vol. 28, no. 4, pp. 426–444, 1957.

[14] J. B. Keller, R. M. Lewis, and B. D. Seckler, "Diffraction by an aperture. II," *J. Appl. Phys.*, vol. 28, no. 5, pp. 570–579, 1957.

[15] L. Brillouin, *Wave Propagation in Periodic Structures. Electric Filters and Crystal Lattices*, ser. International Series in Pure and Applied Physics. New York: McGraw-Hill, 1946.

[16] Ansoft, "High-Frequency Structure Simulator: High Frequency Electromagnetic Simulator Ansoft. Pittsburgh, PA, 2006 [Online]. Available: http://www.ansoft.com/products/hf/hfss/

Ehsan Afshari was born in Tehran, Iran, in 1979. He received the B.Sc. degree in electronics engineering from the Sharif University of Technology, Tehran, Iran, and the M.S. and Ph.D. degrees in electrical engineering from the California Institute of Technology, Pasadena, in 2003, and 2006, respectively.

In August 2006, he joined the faculty in Electrical and Computer Engineering, Cornell University, Ithaca, NY. His research interest is the application of the mathematical theory of wave propagation to high performance circuit design.

Dr. Afshari was awarded DARPA's Young Faculty Award in 2008 and nation's Best Engineering Student award by the President of Iran in 2001. He is also the recipient of the best paper award in the Custom Integrated Circuits Conference (CICC), September 2003, the first place at Stanford-Berkeley-Caltech Inventor's Challenge, March 2005, the recipient of the Silver Medal in the Physics Olympiad in 1997, and the recipient of the "Award of Excellence in Engineering Education" from Association of Professors and Scholars of Iranian Heritage (APSIH), May 2004.

Harish S. Bhat received the A.B. degree in mathematics from Harvard University, Cambridge, MA, in 2000 and the Ph.D. degree in control and dynamical systems from California Institute of Technology, Pasadena, in 2005.

From 2005 to 2007, he held the Chu Assistant Professorship in Applied Mathematics at Columbia University, New York, NY. In 2008, he joined the faculty of the School of Natural Sciences at the University of California, Merced, the tenth and newest campus in the UC system. His research interests include the study of wave propagation using a variety of mathematical techniques from dynamical systems, partial differential equations, and numerical analysis. Waves in discrete, dispersive, and/or nonlinear media are all of interest, as are waves whose governing equation can be associated to a Hamiltonian or Lagrangian structure.

Ali Hajimiri received the B.S. degree in electronics engineering from the Sharif University of Technology, Tehran, Iran, and the M.S. and Ph.D. degrees in electrical engineering from the Stanford University, Stanford, CA, in 1996 and 1998, respectively.

He was a Design Engineer with Philips Semiconductors, where he worked on a BiCMOS chipset for GSM and cellular units from 1993 to 1994. In 1995, he was with Sun Microsystems, where he worked on the UltraSPARC microprocessor's cache RAM design methodology. During the summer of 1997, he was with Lucent Technologies (Bell Labs), Murray Hill, NJ, where he investigated low-phase-noise integrated oscillators. In 1998, he joined the Faculty of the California Institute of Technology, Pasadena, where he is an Associate Professor of Electrical Engineering and the director of Microelectronics and Noise Laboratories. His research interests are high-speed and RF integrated circuits. He is a coauthor of *The Design of Low Noise Oscillators* (Kluwer, 1999) and holds several U.S. and European patents. He is a cofounder of Axiom Microdevices Inc.

Dr. Hajmiri is an Associate Editor of the IEEE JOURNAL OF SOLID-STATE CIRCUITS (JSSC) and a member of the Technical Program Committee of the International Solid-State Circuits Conference (ISSCC). He has also served as an Associate Editor of IEEE TRANSACTIONS ON CIRCUITS AND SYSTEMS—II: EXPRESS BRIEFS, a member of the Technical Program Committees of the International Conference on Computer Aided Design (ICCAD), Guest Editor of the IEEE TRANSACTIONS ON MICROWAVE THEORY AND TECHNIQUES, and the Guest Editorial Board of Transactions of Institute of Electronics, Information and Communication Engineers of Japan (IEICE). He was selected to the top 100 innovators (TR100) list. He was the Gold medal winner of the National Physics Competition and the Bronze Medal winner of the 21st International Physics Olympiad, Groningen, Netherlands. He was a co-recipient of the International Solid-State Circuits Conference (ISSCC) 1998 Jack Kilby Outstanding Paper Award and a three times winner of the IBM faculty partnership award as well as National Science Foundation CAREER Award.